ELSEVIER

Journal of Electrostatics 46 (1999) 91–101

Journal of
ELECTROSTATICS

Real time optical correction using electrostatically actuated MEMS devices

M. Horenstein[a], T. Bifano[b], S. Pappas[a], J. Perreault[a], and R. Krishnamoorthy-Mali[b]

[a]Dept. of Electrical and Computer Engineering, Boston University, 8 Saint Mary's St., Boston, MA, 02215 USA (e-mail:mnh@bu.edu)

[b]Dept. of Aerospace and Mechanical Engineering, Boston University, 110 Cummington St., Boston, MA, 02215 USA

This paper describes an optical correction system made from electrostatically actuated, surface machined micro-electromechanical (MEMS) mirrors. Such MEMS mirrors have applications in optical systems where they are used to correct wavefront aberrations and other image distortions. In our experiments, electrostatic actuators having a maximum surface-normal stroke of 2.5 μm control the individual orientations of each element in an array of 300-μm square mirror segments in the tip-tilt mode. Real time correction of random optical aberrations is demonstrated using a single mirror segment with four independently mounted corners and closed-loop feedback control.

1. INTRODUCTION

Deformable mirrors based on micro-electromechanical (MEMS) technology have been investigated by several research groups as an inexpensive and high-performance alternative to more conventional piezoelectrically actuated deformable mirrors. Previous research has focused on continuous membrane, bulk-micromachined modal mirrors [1,2] and surface-micromachined, piston-motion segmented mirrors [3]. This paper describes an alternative system that represents a compromise between these two very different competing technologies. Specifically, we are currently developing an array of corner-mounted segmented mirrors with tip-tilt movement for use in optical image correction.

2. BASIC ACTUATOR

The electrostatic actuator upon which our mirror systems are based is shown in Fig. 1. The properties of this device have been described in detail in several previous papers [4-6], hence only a brief summary of their operation is provided here. The double cantilever structure of Fig. 1, sometimes called the "fixed-fixed end" actuator, is fabricated on a silicon wafer substrate using standard surface micromachining methods. It consists of a 2-μm thick flexible polysilicon diaphragm suspended by two rigid walls above a stationary polysilicon actuation electrode. The latter is separated from the silicon substrate by a 0.5-μm thick insulating silicon-nitride layer, thus permitting voltage to be applied to the electrode. In our devices,the gap between the diaphragm and the actuation electrode is about 5 μm, and the typical planar dimensions of the diaphragm fall in the range 100 to 350 μm.

0304-3886/99/$ – see front matter
PII: S0304-3886(99)00015-7

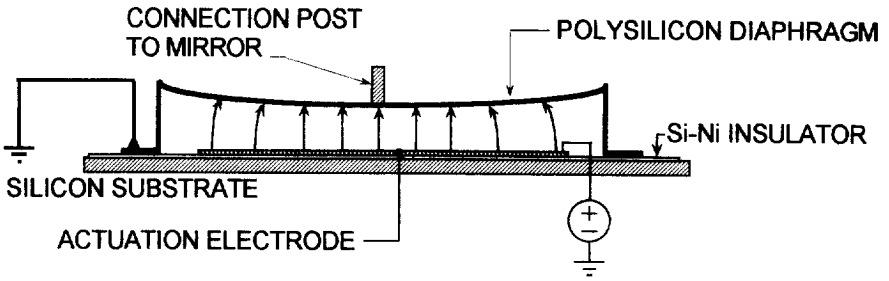

Figure 1 - Basic double-cantilevered (fixed-fixed end) electrostatic MEMS actuator used in optical mirror experiments. Applying a voltage to the actuation electrode causes the diaphragm to deflect toward the substrate.

Under normal operation, the flexible diaphragm is held at ground potential. A voltage is applied to the actuation electrode, causing an electric field to develop in the air gap. The resulting electrostatic force causes the diaphragm to deflect toward the substrate until the electrostatic force is balanced by the counteracting mechanical force. The 5-μm gap spacing of our devices lies well below the minimum of the Paschen breakdown curve [7], so that very high electric fields and force densities can be achieved without air breakdown or sparking. In air at atmospheric pressure, a 5 μm gap can support electric fields as high as about 70 V/μm [8,9], corresponding to actuator voltages of up to 350 V.

Obtaining precise solutions for the electrostatic force density acting on the diaphragm and the diaphragm's deflection profile can be a difficult task. One must perform a detailed analysis of both the mechanical deformation of the diaphragm and the field distribution inside the air gap. The field distribution and mechanical deformation are coupled, hence such analyses invariably involve numerical modeling using finite element methods. Computations of this type have been the subject of several MEMS-related papers [10-13]. In many situations, however, a first-order qualitative *estimate* of diaphragm behavior is all that is required. One can be found by adopting a lumped element approach and assuming the diaphragm and electrode to behave like a simple, mechanically suspended parallel plate capacitor of value

$$C = \epsilon_0 A/(g - y) \tag{1}$$

where g is the actuator gap spacing at zero voltage, y the deflection from rest measured in the center of the diaphragm, and A the diaphragm area. This simplified expression neglects edge effects as well as field perturbations due to the curvature of the diaphragm as it deforms toward the substrate and underestimates the total integrated force on the diaphragm by a factor on the order of about 10-20% [5].

The total electrostatic force acting on the diaphragm as a function of deflection can be found by taking the derivative with respect to y of the stored capacitive energy $E = CV^2/2$ at constant voltage [14]. If diaphragm curvature is ignored, i.e., if small diaphragm deflections are assumed equivalent to uniform displacement y, then the electrostatic force becomes

$$F_e = \frac{V^2}{2}\frac{dC}{dy} = -\frac{V^2\epsilon_0 A}{2(g-y)^2} \tag{2}$$

For small deflections, the total mechanical force acting on the diaphragm can be modeled as a linear lumped-element restoring force $F_m = -ky$. The equilibrium position of the diaphragm under constant voltage V will be the value of y at which $F_e + F_m = 0$. Because F_e varies as $1/y^2$ and F_m as y, the deflection vs voltage relation becomes a cubic equation of the form

$$y(g-y)^2 = V^2\epsilon_0 A/2k \tag{3}$$

As discussed in several references [2,4,5,10,11], a double-cantilevered MEMS actuator obeying this equation (or refined versions derived from more detailed analyses) becomes unstable above a threshold "snap through" voltage at which dy/dV becomes infinite. At the snap-through voltage, the magnitude of the electrostatic force F_e begins to increase with deflection more rapidly than the magnitude of the mechanical restoring force F_m. The onset of snap-through instability leads to a complete collapse of the actuator gap as the diaphragm snaps to the substrate. Although a reversible effect, snap through represents a limiting, self-latching, hysteresic state of the actuator and is avoided in systems designed for continuously variable motion. Actuators in optical imaging systems typically are biased at a point lying between zero deflection and the onset of snap-through instability. In this biased regime of operation, diaphragm deflection increases monotonically with applied voltage.

In our previous experiments [4,5,6], actuators and mirrors were fabricated using standard semiconductor processing steps offered by MCNC under its multiuser MUMPS program [15]. In the work reported here, prototype mirrors were fabricated using a custom-designed three-layer polysilicon surface micromachining process. In this process, polysilicon serves as the structural material, phospho-silicate glass (PSG) as the sacrificial material, and silicon nitride as an electrical isolation layer separating the actuation electrodes from the underlying substrate. Most surface micromachined MEMS processes make use of sacrificial material such as PSG to build up three dimensional structures. These sacrificial layers are later etched away to form gaps and spaces between mechanical components. In our devices, for example, sacrificial PSG was used to fill the gaps under the diaphragms during fabrication but was later dissolved by hydrogen fluoride to create the air gap regions.

Surface micromachined devices usually include small holes in large structural polysilicon layers to allow dissolving etchants to properly reach all the sacrificial material. In optical structures, however, such holes ruin the optical planarity of the outer mirror layer. In our devices, liquid access to the sacrificial PSG layer was provided by first anisotropically etching holes from the *back* of the wafer all the way through the substrate. This method allowed us to avoid small holes in the mirror surface while helping to preserve the optical planarity of the mirror surface.

Figure 2 shows voltage versus deflection curves for several actuators of various sizes. These curves have the basic form of Eq. (3). Deflection was measured using a Zygo laser-doppler position measuring system. The maximum observed deflection before snap-through (not shown on the plots) was approximately 2 to 2.5 μm. This deflection limit defines the maximum usable stroke distance for controlling optical mirrors. A dynamic study showed the actuators to have a mechanical frequency response bandwidth greater than 70 kHz.

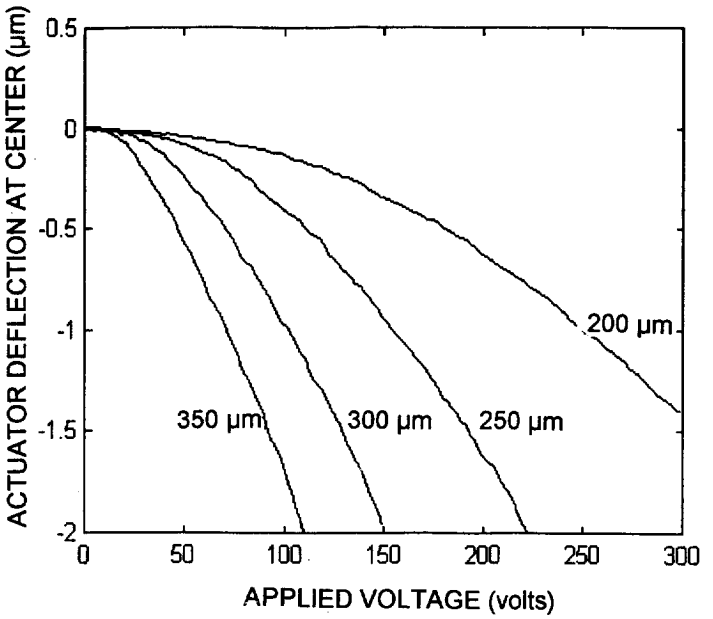

Figure 2 - Measured deflection versus voltage for electrostatic fixed-fixed actuators of various sizes.

3. TIP-TILT MIRROR SYSTEM

In the present work, the electrostatic actuator structure of Fig. 1 has been incorporated into a deformable mirror system of the tip-tilt type. As depicted in Fig. 3, square mirror segments are supported at each corner by underlying double-cantilevered electrostatic actuators. Each actuator is prebiased to a set deflection with an offset voltage. Applying an additional differential-mode signal to the actuators supporting opposite corners of a mirror causes that mirror to "tip" about its x-axis or "tilt" about its y-axis. Adjacent mirror segments share actuators, so that each actuator controls four nearest-neighbor mirror corners. The actuators provide precise control of each mirror's attachment points in the surface-normal direction. The typical actuator is constructed from a 300 μm-square deformable membrane spaced at a 350 μm center-to-center distance from adjacent actuators. The segmented, tip-tilt mirror system of Fig. 3 represents a compromise between two alternative systems. One alternative utilizes fully isolated mirror segments each singly supported in the center by its own actuator. In this so-called "piston mirror" system, each mirror segment is totally uncoupled from its neighbors. Adjacent actuators exhibit no inter-actuator coupling, allowing for much simpler control algorithms in optical image systems. Undesirable diffraction may occur, however, due to the step discontinuities at the segment edges. At the same time, only the surface-normal position of the actuator can be controlled; no tip or tilt is possible. A second alternative consists of a fully continuous deformable mirror membrane supported at many points by multiple actuators. Continuous mirrors offer the advantage of full contour control and no surface discontinuities but require complicated control algorithms to account for the complex inter-actuator coupling effects caused by the mechanical properties of the membrane. In the segmented mirror systems developed in our experiments, the only coupling between

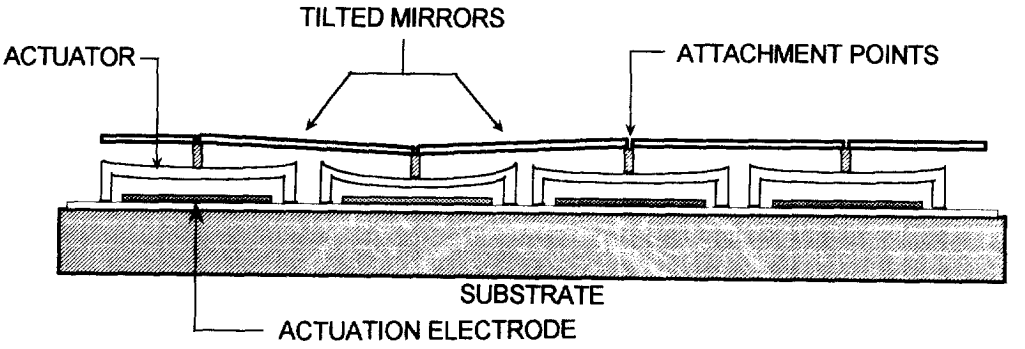

Figure 3 - Actuator array supports the corners of tip-tilt mirror segments. Differential-mode signals cause each mirror to "tip" about its x-axis or "tilt" about its y-axis.

segments is via corner position, i.e. no coupling via the mirror segments occurs, but step discontinuities between mirror segments are eliminated.

4. REAL TIME OPTICAL CORRECTION

In adaptive optics (AO) systems, deformable mirrors are used as active elements for changing the direction of propagation of incoming rays of light. This technique, called *phase aberration correction*, allows images distorted during propagation to be restored to clarity. Image distortion can occur due to a variety of effects, including turbulence, thermal currents, or diffraction from airborne dust particles. Applications of AO systems include astronomy, medical imaging, target recognition, and optical correlation. The aberrated wave to be corrected is first sent to a sensor which optically analyzes each area sector of the wavefront plane for direction of propagation. The output of the wavefront sensor is used to control and distort the surface of the deformable mirror which then corrects the direction of propagation of each sector of the wavefront plane to compensate for the optical aberration.

The ultimate goal of our experiments is to produce a multiple segment, fully deformable mirror for optical image correction. As a preliminary step, we have performed a simple experiment to demonstrate that our MEMS mirror devices can indeed be used for dynamic optical wavefront correction. Figure 4 shows the experimental setup. A collimated, 4-mW helium-neon (HeNe) laser beam was focussed onto one segment of a tip-tilt MEMS mirror array of the type depicted in Fig. 3. A random, dynamic optical aberration was introduced by placing a candle flame under the laser beam path. The heat from the flame produced distorting thermal currents. The length scale of the turbulence was much larger than the beam diameter, so that the effect of the aberration was to completely change the direction of propagation of the beam. A two-axis, differential photodetector was used to determine the exact position of the beam after reflection from the MEMS mirror. Such a detector contains four planar, pie-shaped photodiodes situated in a circle whose plane is perpendicular to the z-axis of the laser beam. Monitoring the two differential outputs of the sensor -- one for the x-axis and one for the y-axis -- allows the location of the centroid of the laser beam to be determined. The signals from the detector were fed to two differential amplifiers (one for each axis of the image plane), amplified, combined with a fixed dc bias, then fed to four high-voltage amplifiers. The outputs of the latter, consisting of differential signals plus bias,

were fed to the actuators supporting the four corners of the tip-tilt mirror segment. Because electrostatic actuators can only be pulled toward the substrate, and not repelled from it, the dc bias was required to permit both positive and negative tilt about an initial bias point. The overall feedback loop, based on simple proportional feedback control, is summarized in Fig. 5. Its purpose was to return the laser beam to the center of the detector aperture in response to random changes in beam direction caused by the candle flame. A summary of the various voltages, gains, and typical signal levels in the system are provided in Table 1.

Table 1 - Parameters and Typical Signal Levels for the Feedback Control System of Fig. 5

Symbol	Description	Value/Range
A_I	current-to-voltage conversion ratio	10^4 V/A
A_d	differential amplifier gain	1
A_1	signal amplifier gain	33
A_H	high voltage amplifier gain	20
V_{BIAS}	dc bias	5 V
$\lvert v_X \rvert$	differential mode signal	4 V
v_{XH}	high voltage signal to actuator	100 ± 80 V

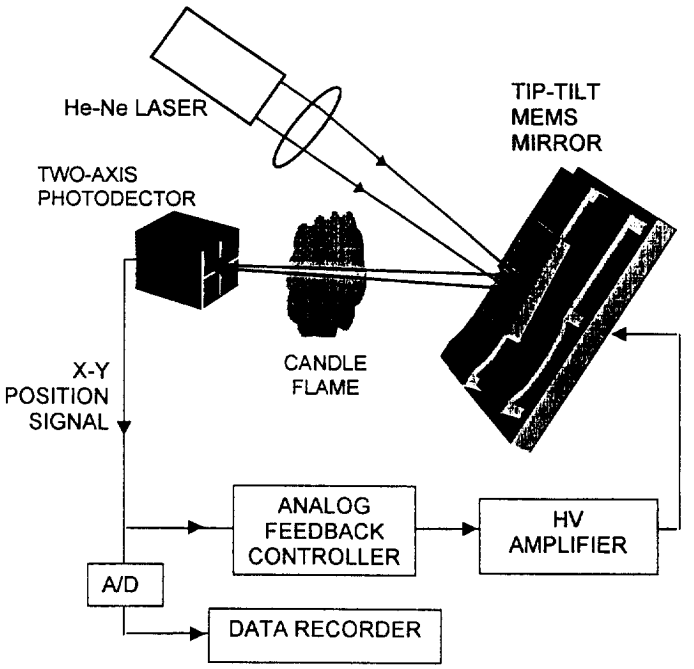

Figure 4 - Experimental setup. The laser beam is perturbed by warm air turbulence from a candle flame. The feedback loop, including MEMS mirror, controller, and high-voltage driver, corrects for the optical aberration.

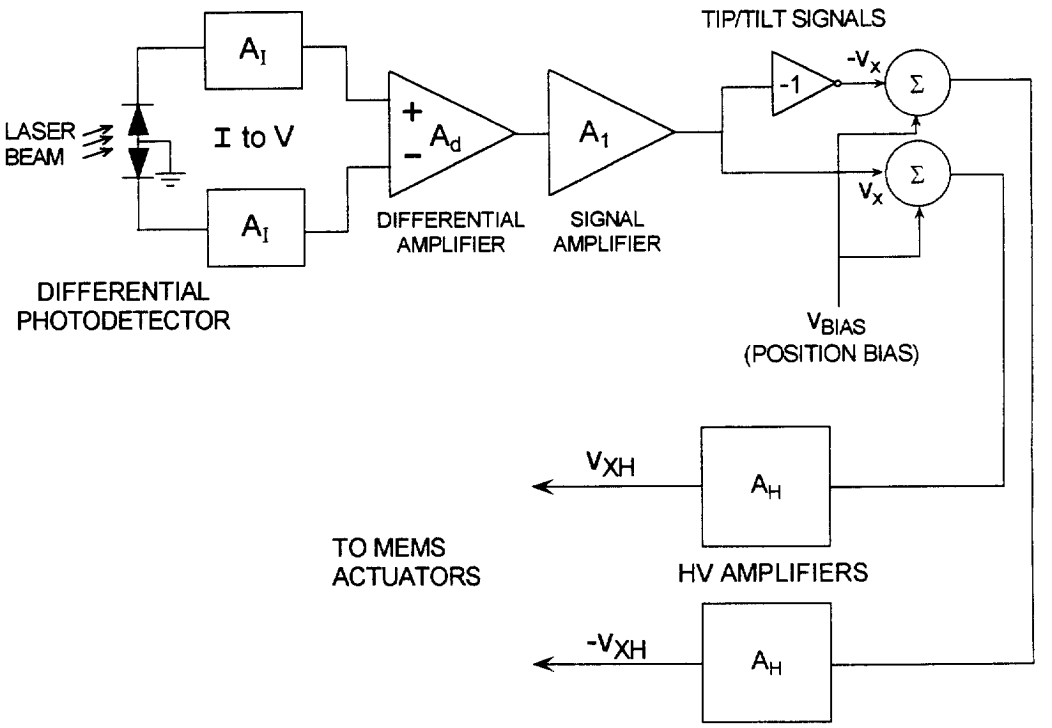

Figure 5 - Feedback control scheme used to correct for aberrations in the optical signal path. Its purpose is to hold the laser beam in the center of the detector aperture.

5. HIGH VOLTAGE AMPLIFIER

One novel feature of our electrostatic control system is the use of a custom-designed optically coupled high voltage amplifier. This circuit was developed to provide a low cost alternative to more expensive, commercially available amplifiers and was designed so that it could be replicated many times (> 100) in a multi-channel MEMS mirror controller without requiring significant part count or circuit board space. The details of the high-voltage amplifier are shown in Fig. 6. The incoming low-voltage signal, buffered by the operational amplifier, drives the light-emitting diode of an opto-isolator. The phototransistor inside the opto-isolator forces current into a resistive divider, providing feedback to the op-amp. The current level through the phototransistor increases until the inverting op-amp input reaches nearly the same voltage as the non-inverting input. For an op-amp of sufficiently high open-loop gain, this feedback-null condition results in an output voltage given by

$$v_{OUT} = (1 + R_2/R_1)v_{IN} \tag{4}$$

where $(1 + R_2/R_1)$ is the high voltage gain. A list of component values and part types is provided in Table 2. These resistor values shown in the table yield a voltage gain of 20.

Table 2
Description of Components for the High Voltage Amplifier of Figure 6.

Symbol	Description	Value/Type
R_1	feedback resistor	10 kΩ (±1%)
R_2	amplification resistor	190 kΩ (±1%)
R_B	current limiting resistor	1 kΩ (±1%)
OP	operational amplifier	LF411
Q_1	opto-isolator (V_{CEO} = 300 V)	H11-D2

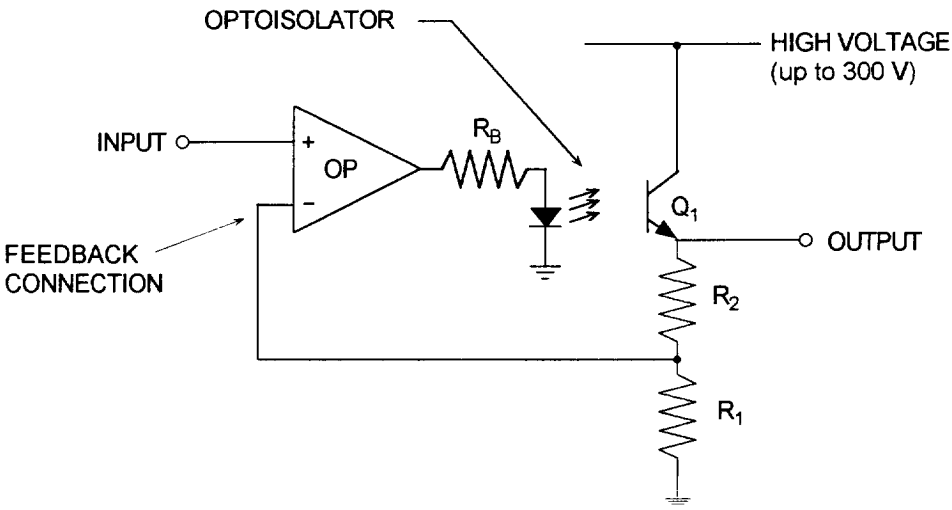

Figure 6 - Basic circuit diagram of the high-voltage amplifier. The output is equal to $(1 + R_2/R_1)$ times the input voltage.

6. EXPERIMENTAL RESULTS:

The optical correction system of Figs. 4 and 5 was tested under both open-loop (no feedback) and negative (full) feedback conditions. With the candle flame distorting the laser beam path, the position of the beam on the face of the photodetector was measured for five seconds with the controller turned off and for five seconds with the controller turned on. Figure 7 shows the locus over time of the laser beam position as measured by the detector

with no feedback control. Figure 8 shows the locus of beam position with full feedback control. In both plots, the beam position has been expressed in terms of an incident angle, or "wavefront tilt," relative to the surface normal of the photodetector. Significant reduction in random deviations of the beam position is evident when the adaptive optics controller is activated.

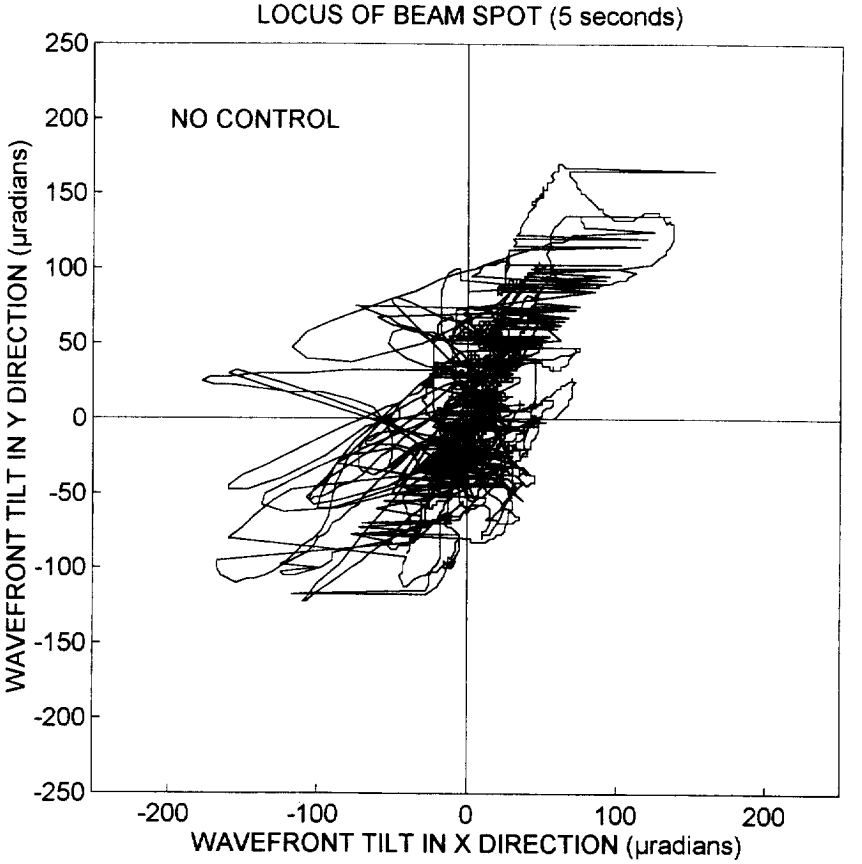

Figure 7 - Locus of beam position over a five second time interval *with no* feedback control. The beam position has been expressed in terms of an incident angle, or "wavefront tilt," relative to the surface normal of the photodetector.

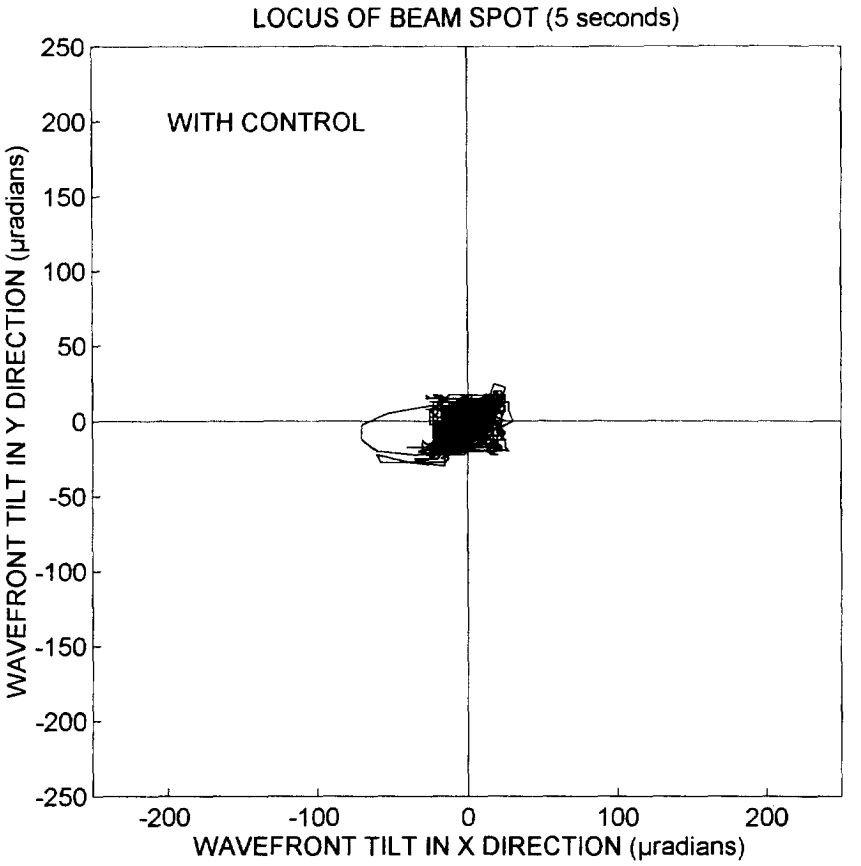

Figure 8 - Locus of beam position over a five second time interval *with* feedback control.

7. DISCUSSION

Control of tip and tilt using a single electrostatically-actuated mirror segment demonstrates the fundamental operations needed to correct more complex wavefront aberrations. In an adaptive optics system based on a large array of MEMS actuators and mirror segments, a more comprehensive wavefront sensor made from a lenslet array, sometimes called a "Hartmann" sensor, can be used to poll multiple sectors of an aberrated wavefront. In such a system, deviations in the local direction of propagation in each wavefront sector translate into shifts in position of the focussed spots produced by the lenslet array. Shifts in spot location can be used to provide correction signals to corresponding actuators of a multi-mirror deformable array, in turn compensating for complicated aberrations in the optical signal path. The single mirror system described in this paper is readily expanded for use in such a multi-mirror adaptive optics system.

8. ACKNOWLEDGMENTS

The authors would like to extend thanks to the Defense Advanced Research Projects Agency (DARPA) for funding this research project and to Asaf Fishov for assistance with the control circuitry.

REFERENCES

1. G. Vdovin, P. Sarro, "Flexible Mirror Micromachined in Silicon," *Appl. Optics*, 34 (1995), pp. 2968-2972.
2. M. Miller, M. Argonin, R. Bartman, W. Kaiser, T. Kenny, R. Norton, E. Vote, "Fabrication and Characterization of a Micromachined Deformable Mirror," *Proc. SPIE 1945,* 1993, pp. 421-430.
3. M. Roggemann, V. Bright, B. Welsh, S. Hick, P. Roberts, W. Cowan, J. Comtois, "Use of Micro-Electromechanical Deformable Mirrors to Control Aberrations in Optical Systems: Theoretical and Experimental Results," *Optical Engineering*, 36 (2), May 1997, pp. 1327-1338.
4. R. Krishnamoorthy Mali, T. Bifano, M. Horenstein, N. Vandelli, "Development of Micro-electromechanical Deformable Mirrors for Phase Modulation of Light," *Optical Engineering*, 36 (2), Feb 1997, pp. 542-548.
5. M.Horenstein, T. Bifano, R. Mali, N Vandelli, "Electrostatic Effects in Micromachined Actuators for Adaptive Optics," *Jour. of Electrostatics,* 42(1-2), Sep 1997.
6. T. Bifano, R. Krishnamoorthy Mali, J. Dorton, J. Perreault, N. Vandelli, M. Horenstein, D. Castañon, "Continuous Membrane, Surface Micromachined, Silicon Deformable Mirror," *Optical Engineering*, 36 (5), May 1997, pp. 1354-1360.
7. J.D. Cobine, *Gaseous Conductors*, New York: Dover Press, 1958.
8. R.M. Schaffert, *Electrophotography*, New York: John Wiley and Sons, 1975, pp. 514.
9. J.M. Crowley, "Dimensionless Ratios in Electrohydrodynamics", in *Handbook of Electro- static Processes*, J.S. Chang, A.J. Kelly, J.M. Crowley, eds. New York: Marcel Dekker, Inc., p. 101.
10. J. R. Gilbert, R. Legtenberg, and S.D. Senturia, "3-D Coupled Electromechanics for MEMS: Applications of CoSolve-EM," *Proceedings MEMS '95,* Amsterdam, July 1995.
11 P. Osterberg, H.Yie, X. Cai, J. White, S. Senturia, "Self Consistent Simulation and Modeling of Electrostatically Deformed Diaphragms", *Proc. MEMS '94,* Oiso, Japan, Jan '94.
12. M.A. Michalicek, V.M Bright, and J.H. Comtois, "Design, Fabrication, Modeling, and Testing of a Surface-Micromachined Micromirror Device", *Proceedings of the ASME,* Dynamic Systems and Control Division, DSC 57-2, 1995.
13. D. Maier-Schneider, J. Maibach, E. Obermeier, "A New Analytical Solution for the Load Deflection of Square Membranes", *Jour. Microelectromechanical Systems,* 4 (4), Dec. 1995.
14. H. Woodson and J.R. Melcher, *Electromechanical Dynamics, Part I: Discrete Systems*. New York: John Wiley and Sons, 1968.
15. D. Koester, R. Mahadevan, K.W. Markus, "MUMPs Introduction and Design Rules", MCNC Technology Applications Center, 3021 Cornwallis Road, Research Triangle Park, NC, Oct. 1994. (http://mems.mcnc.org/mumps.html).